UCSF

Title

Left ventricular myocardial contractility is depressed in the borderzone after posterolateral myocardial infarction.

Permalink

https://escholarship.org/uc/item/2d93s67k

Journal

Authors

Shimkunas, Rafael
Zhang, Zhihong
Wenk, Jonathan
et al.

Publication Date

DOI

Left ventricular myocardial contractility is depressed in the borderzone after postero-lateral myocardial infarction

Rafael Shimkunas, MS[4,6], **Zhihong Zhang, MS**[6], **Jonathan F. Wenk, PhD**[6], **Mehrdad Soleimani, MD**[6], **Michael Khazalpour, MD**[6], **Gabriel Acevedo-Bolton, PhD**[6], **Guanying Wang, MD, PhD**[6], **David Saloner, PhD**[5,6], **Rakesh Mishra, MD**[4,6], **Arthur W. Wallace, MD, PhD**[2,6], **Liang Ge, PhD**[1,3,6], **Anthony J. Baker, PhD**[4,6], **Julius M. Guccione, PhD**[1,3,6], and **Mark B. Ratcliffe, MD**[1,3,6,*]

[1]Department of Surgery, University of California, San Francisco, CA

[2]Department of Anesthesia, University of California, San Francisco, CA

[3]Department of Bioengineering, University of California, San Francisco, CA

[4]Department of Medicine, University of California, San Francisco, CA

[5]Department of Radiology, University of California, San Francisco, CA

[6]Department of Veterans Affairs Medical Center, San Francisco, CA

Abstract

Background—Contractility in the borderzone (BZ) after antero-apical myocardial infarction (MI) is depressed. We tested the hypothesis that BZ contractility is also decreased after postero-lateral MI.

Methods—Five sheep underwent postero-lateral MI. Magnetic resonance imaging (MRI) was performed 2 weeks before and 16 weeks after MI, and left ventricular (LV) volume and regional strain were measured. Finite element (FE) models were constructed and the systolic material parameter, T_{max}, was calculated in the BZ and remote myocardium by minimizing the difference between experimentally measured and calculated LV strain and volume. Sheep were sacrificed 17 weeks after MI and myocardial muscle fibers were taken from the BZ and remote myocardium. Fibers were chemically demembranated, and isometric developed force, F_{max}, was measured at supra-maximal $[Ca^{2+}]$. Routine light microscopy was also performed.

Results—There was no difference in T_{max} between pre-MI and remote myocardium 16 weeks after MI. However, there was a large decrease (63.3%, p=0.005) in T_{max} in the BZ when compared with the remote myocardium 16 weeks after MI. In addition, there was a significant reduction of BZ F_{max} for all samples (18.9%, p=0.023). Myocyte cross-sectional area increased by 61% (p=0.021) in the BZ, but there was no increase in fibrosis.

Conclusion—Contractility in the borderzone is significantly depressed relative to the remote myocardium after postero-lateral MI. The reduction in contractility is due at least in part to a decrease in contractile protein function.

Keywords

myocardial infarction; remodeling; borderzone; ventricular function; cardiac mechanics; contractility; magnetic resonance imaging; finite element

Corresponding Author: Mark B. Ratcliffe, MD, Surgical Service (112), Veterans Affairs Medical Center, 4150 Clement Street, San Francisco, CA 94121, Telephone: (415) 221-4810 x 2962, mark.ratcliffe@va.gov.

Introduction

It has been known since the mid-1980s that systolic performance (systolic shortening and wall thickening) is depressed in the non-ischemic borderzone (BZ) after antero-apical myocardial infarction (MI). [1] It was initially thought that the reduced BZ function was due to mechanical tethering by the infarct. However, finite element (FE) -based inverse calculations of regional contractility, in which optimization routines attempt to match computed and experimentally measured LV volume and strain, suggest that BZ contractility is reduced by more than 50%. [2] Moreover, BZ contractility appears to vary linearly across the BZ and the BZ may be as much as 3 cm in width after antero-apical MI. [3]

Myocardial infarction involving the postero-lateral or inferior LV wall behaves differently than MI of the antero-apical LV wall. Postero-lateral MI is less likely to undergo expansion, [4] and survival after postero-lateral MI is increased. [5] In addition, chronic ischemic mitral regurgitation (CIMR) is caused by LV remodeling after postero-lateral MI in which the posterior papillary muscle moves laterally. [6, 7] It is therefore possible that the reduction in BZ contractility after postero-lateral MI is different than after antero-apical MI and that LV remodeling and development of ischemic mitral regurgitation may be affected.

The purpose of this study was twofold. First, we determined contractility (systolic material parameter, T_{max}) in the BZ and remote myocardium in sheep after postero-lateral MI using magnetic resonance imaging (MRI) -based inverse finite element methods. Second, maximum isometric developed force was measured *in vitro* in myocardial samples from the BZ and remote myocardium. We tested the hypothesis that there is a significant depression in contractility in the infarct BZ relative to remote myocardium after postero-lateral MI.

Methods

The sheep used in this study were treated in compliance with the "Guide for the Care and Use of Laboratory Animals" prepared by the Institute of Laboratory Animal Resources, National Research Council, and published by the National Academy Press (revised 1996).

Myocardial infarction

Five male adult Dorset sheep underwent postero-lateral MI as previously described. [8]

Magnetic resonance imaging

Two weeks before and 16 weeks after MI, cardiac MRI with non-invasive tags was performed as previously described. [9] Endocardial and epicardial surfaces of the LV and right ventricles (RV) were contoured (iContours, Liang Ge, Cardiac Biomechanics Lab, San Francisco, CA) as well as the stroke volumes of the LV and RV as previously described. [10]

Calculation of 3D myocardial strain

Calculation of systolic strain has been previously described. [11] Briefly, tag lines were segmented (FindTags, Laboratory of Cardiac Energetics, National Institutes of Health, Bethesda, MD) in each MRI image slice (Figure 1) [12] and systolic myocardial strains were calculated at mid-wall and around the circumference in each short-axis slice from tag-line deformation using a four dimensional, B-spline-based motion tracking technique (TTT; Laboratory of Cardiac Energetics, Bethesda, MD). [13]

Finite element models

Finite element models of the LV were created as previously described. [14] Briefly, finite element models were created using early diastole as the unloaded reference configuration (Figure 2). The infarct region was determined from the post-mortem digital photograph. The BZ extended 1 cm in width from the infarct edge. Cardiac myofiber angles and boundary conditions were assigned as previously described. [14]

Material properties

Nearly incompressible, transversely isotropic, hyperelastic constitutive laws for passive [15] and active myocardium [16] were modeled in a user-defined material subroutine an explicit FE solver (LS-DYNA, Livermore Software Technology Corporation, Livermore, CA). The diastolic constitutive laws and the diastolic material parameters used have been previously described. [2]

Systolic material parameters

Kim and colleagues found Ca^{2+} transient amplitude (in Fura-2 ratio units) in the BZ and remote myocardium to be 1.08 and 0.69 respectively 8 weeks after antero-apical MI in sheep. [17] Along those lines, we assigned $Ca_0 = 1$ μmol/L for remote zone and $Ca_0 = 0.65$ μmol/L for the BZ. Other material constants for active contraction were assumed to be: $t = 25$ ms (end systole), $(Ca_0)_{max} = 4.35$ μmol/L, $B = 4.75$ μm^{-1}, $l_0 = 1.58$ μm, $m = 1.0489$ sec μm^{-1}, $b = -1.429$ sec, and l_R was set at 1.85 μm. [18]

Systolic material parameter optimization

The systolic material parameter, T_{max}, was calculated in the BZ and remote myocardium by minimizing the difference between experimentally measured and calculated LV strain and volume. The details of the optimization routine used in this study have been previously described. [19]

Post-hoc adjustment of Tmax

After optimization was complete, the C_t parameter in Sun et al, Equation 6, was factored out by setting $T_{max} = T_{max} C_t$ [2] This was done in order to match the form of the modified Hill equation and allow more direct comparison with skinned fiber developed force, F_{max}.

Post-mortem examination

Sheep were sacrificed one week after the 16 week MRI. The heart was excised. Cardiac arrest was rapidly achieved by retrograde ascending aortic infusion of a cold hyperkalemic solution (Plegisol, Hospira Inc, Lake Forest, IL; 1 L plus 10 mL of 8.4% $NaHCO_3$ at 4 °C to achieve pH 7.8 at room temperature). The right ventricle was removed. The LV was opened by incising the septum and the anterior leaflet of the mitral valve. A digital photograph was taken of the LV endocardium. A transmural strip of myocardium (approximately 2×6 cm) extending circumferentially from the infarct to the posterior wall was excised from the LV. BZ and remote myocardium regions were defined as 0–1 cm and 3–4 cm from the infarct edge, respectively.

In vitro myofilament contractility

Epicardial muscle fibers from BZ and remote myocardium were pinned on silicone substrate at approximate physiological sarcomere length and chemically skinned in a relaxing solution with 1% Triton® X-100 (Sigma Aldrich, St. Louis, MO) for 24 h at 4 °C. [20] Following chemical treatment, samples were washed in relaxing solution for 2 hours at 4 °C and then stored in a 1:1 solution of relaxing solution plus glycerol at −20 °C.

Measurement of developed force in skinned myocardial fibers was performed as previously described. [21] Measurements were performed with a permeabilized fiber test system (Model 1400A, Aurora Scientific, Inc., Ontario, Canada). Early samples (n=3) were measured at a passive tension of 0.98 mN/mm^2 and sarcomere length was not measured. In later experiments (n=2) sarcomere length was measured by laser diffraction and measurements were performed at a sarcomere length of 2.1 μm. Samples were initially bathed in relaxing and pre-activating solutions before immersion in an activating solution with supra-maximal [Ca^{2+}]. F_{max} was normalized to muscle cross-sectional area (mN/mm^2). [21]

Histology

Freshly isolated samples from the BZ and remote myocardium were fixed in phosphate-buffered 4% paraformaldehyde (Fisher Scientific, Inc., Fair Lawn, NJ) at 4 °C for at least 24 h. Paraffin-embedded thick sections were stained with hematoxylin and eosin (H&E) and picrosirius red as previously described. [22] Images of stained cross-sections were analyzed using ImageJ (NIH, Bethesda, MD). Segmentation of myocytes was performed on cells containing only visible nuclei to ensure the representative cross-sectional area along the cell length. Collagen content in picrosirius red-stained sections was quantified using ImageJ thresholding analysis for collagen-positive areas.

Statistical analysis

All values are expressed as mean ± standard deviation (SD). Multivariable mixed model regression was performed (SAS system for Windows Version 9.1, SAS Institute, Cary, NC). Individual comparisons of T_{max} and F_{max} were performed with paired t-tests.

Results

LV pressure and volume before and 16 weeks after postero-lateral MI is shown in Table 1. Although LV pressure at ED and ES are unchanged, LV volumes at both ED and ES are increased (24.4%, p=0.1522 and 50.2%, p=0.0788 respectively). Although LV EF is decreased by 15.6% (p=0.0954), total LV stroke volume is unchanged. However, because there is moderate ischemic mitral regurgitation, forward or RV stroke volume is decreased by 28.4% (p=0.033).

Regional circumferential strain before and after MI is seen in Table 2. In general, the FE-predicted systolic strains were in good agreement with the *in vivo* measured strains (Figure 3).

Finite element simulation results

The optimized systolic material parameter, T_{max}, for pre- and post-MI sheep by region is seen in Figure 4. There was no difference in T_{max} between pre-MI and remote myocardium 16 weeks after MI. However, there was a large decrease (63.3%, n=5, p=0.005) in T_{max} in the BZ when compared with the remote myocardium 16 weeks after MI.

Myocardial skinned fiber force

Regional F_{max} after MI is seen in Table 3. F_{max} obtained from samples tested at fixed passive tension showed a reduction in the BZ of 19.9% (n=3, p=0.029) when compared with remote myocardium. F_{max} obtained from samples tested at fixed sarcomere length showed the reduction in the BZ to be 17.0% (n=2, p=0.086) when compared with remote myocardium. There was a significant reduction of BZ F_{max} for all samples (18.9%, n=5, p=0.023). T_{max} and F_{max} normalized to remote myocardium are seen in Figure 5.

Quantitative analysis of histology

Analysis of representative cross-sectional myocardial slices reveals significant myocyte hypertrophy in the BZ, with the mean BZ myocyte cross-sectional area (CSA) of 190.8 ± 21.2 μm (n=2) compared with remote myocardium of 118.5 ± 2.9 μm (n=2), corresponding to a 61% increase in BZ myocyte CSA (p=0.021). Picrosirius red staining of histological sections shows no replacement fibrosis that could account for the reduction in myocardial force (Figure 6). Image analysis shows no significant change in collagen content, with collagen as a percent of total cross-sectional area to be 5.1 ± 0.3% in the BZ and 5.0 ± 0.4% in the remote myocardium (n=2, p=ns).

Discussion

The principal finding of this study is that contractility in the borderzone (BZ) is substantially depressed when compared with the remote myocardium after postero-lateral MI in the sheep. Developed force measured in isolated skinned fibers is also substantially depressed in the infarct BZ, suggesting that contractile protein dysfunction is at least partially responsible for the observed reduction in BZ contractility.

Calculation of myocardial material properties using the inverse finite element method

Recently, we developed and validated a computationally efficient method of material parameter optimization. [19] Those methods hold peak intracellular calcium, calcium sensitivity, and sarcomere length constant and only allow the peak force generation capability of myocytes, T_{max}, to vary. Such an arrangement necessarily redistributes the effect of other factors that might affect contractility into T_{max}. For instance, Ca^{2+} transient amplitude and calcium handling protein levels, [17] as well as intracellular phosphocreatine-to-ATP ratio, [23] are reduced in the BZ after MI and may affect contractile ability. As a consequence, FE-based calculation of T_{max} is not directly comparable to the experimentally measured F_{max}. However, the fact that both the finite element predicted and experimentally measured results showed a depression of myocyte force generation capability is very reassuring.

Our finite element models assume that the BZ region is 1 cm in width. However, finite element models [3] and preliminary experimental data from sheep after antero-apical MI (data not shown) suggest that the BZ may be as wide as 3 cm and that there is a linear F_{max} gradient between the infarct and the base of the heart. These findings suggest that the region of contractile force reduction is larger than previously thought. It should be noted that a large BZ with reduced contractile function is an attractive therapeutic target and that a recent finite element study of enhanced BZ function suggests that even partial improvement of BZ contractility is sufficient to improve pump function. [24]

Comparison of antero-apical and postero-lateral BZ contractility

Our study did not directly compare BZ contractility after poster-lateral MI with BZ contractility after antero-apical MI. However, the 63.3% reduction in BZ T_{max} seen in the current study is similar to the 49.4% reduction in BZ T_{max} after antero-apical MI in our previous study by Sun et al. [2] Further work is needed but it appears that post-MI BZ dysfunction is independent of the MI location.

Contractile protein function

The finding that F_{max} in the BZ was decreased by nearly 20% suggests that contractile protein dysfunction is at least in part responsible for the observed reduction in BZ contractility. The skinned fiber preparation is a robust experimental method that has been used to investigate the underlying mechanisms of contractile dysfunction in skeletal and

cardiac muscle. [25, 26] Skinned fiber measurements are important since they specifically exclude the effects of myocyte calcium handling machinery, permitting bath ion concentrations to be tightly controlled and allowing calcium to directly activate cross-bridge cycling. Skinned fiber measurements provide experimental evidence of dysfunction at the contractile protein level.

While the tests performed at fixed passive tension and fixed sarcomere length differ in magnitude, the proportion of BZ force to remote myocardium remains consistent at approximately 80%. This observation is further demonstrated in experiments (data not shown) where F_{max} was measured for BZ and remote myocardium at decreasing sarcomere lengths (2.1, 2.0, 1.9, 1.8 and 1.7 μm), maintaining a BZ-to-remote myocardium ratio of $84.9 \pm 2.4\%$. These results suggest the proportional reduction of BZ force is similar and independent of sarcomere length.

The mechanism of reduced contractile protein function is unclear but is likely mediated by high stress and strain in the BZ myocardium. We know that strain is altered in the BZ after postero-lateral MI. For instance, Rodriguez and colleagues found that longitudinal strain was decreased [27] and radial-circumferential shear strain was increased in the functional BZ early after circumflex coronary artery occlusion in the sheep. [27, 28] High systolic stress and positive strain in the BZ activates MMPs 2 and 9 [29, 30] and MMP-2 has been shown to directly damage the intracellular contractile proteins myosin light chain 1 and troponin I. [31, 32] Cleavage of such contractile proteins can affect cross-bridge dynamics and should result in reduced myocardial contractility.

Limitations

There are several limitations in the present study. As above, the accurate measurement of intracellular calcium and ECa_{50} values is clearly needed. Second, experiments using chemically skinned fiber experiments performed at a fixed passive tension likely had a sarcomere length less than 2.1 μm. Despite demonstrating the preserved BZ-to-remote myocardium ratio for all samples, future experiments should be conducted at an initial diastolic sarcomere length of 2.1 μm.

Finally, comparison between FE based calculations and experimental measurements would be facilitated by using an active contraction material property law that more closely conforms to underlying biophysical mechanisms. The active contraction law described by Guccione and colleagues, that was used in the current study, has proved invaluable in the analysis of left ventricular mechanics after MI [19] and after application of devices designed to correct heart failure. [33, 34] However, the largely phenomenologic nature of that material property law, that was made necessary by the limited computational power available in 1995, is an increasing limitation. Recently, Rice and colleagues have developed a computationally efficient, active contraction material property law that directly models myocardial action potentials, intracellular calcium transients, and contractile protein cross bridge formation. [35] The ready availability of cheap parallel processing makes the development of a multi-scale model, in which a material law of the Rice type is coupled with optimization of systolic material parameters, both possible and highly desirable.

Conclusion and future directions

Contractility in the borderzone (BZ) is substantially depressed compared with remote contractility in the remote zone after postero-lateral MI in the sheep. Developed force in isolated skinned myofibers is also depressed in the infarct BZ suggesting that decreased contractile protein function is at least in part responsible for the observed reduction in BZ contractility.

Treatment aimed at the prevention or reduction in loss of BZ contractility may significantly improve ventricular pump function. As above, recent finite element based simulations suggest that even a moderate increase in BZ contractility will have a beneficial effect. [24]

Acknowledgments

References

1. Homans DC, Asinger R, Elsperger KJ, Erlien D, Sublett E, Mikell F, et al. Regional function and perfusion at the lateral border of ischemic myocardium. Circulation. 1985; 71(5):1038–1047. [PubMed: 3986974]

2. Sun K, Zhang Z, Suzuki T, Wenk JF, Stander N, Einstein DR, et al. Dor procedure for dyskinetic anteroapical myocardial infarction fails to improve contractility in the border zone. J Thorac Cardiovasc Surg. 2010; 140(1):233–239. 239 e1-4. [PubMed: 20299030]

3. Lee LC, Wenk JF, Klepach D, Zhang Z, Saloner D, Wallace AW, et al. A novel method for quantifying in-vivo regional left ventricular myocardial contractility in the border zone of a myocardial infarction. J Biomech Eng. 2011; 133(9):094506. [PubMed: 22010752]

4. Pirolo JS, Hutchins GM, Moore GW. Infarct expansion: pathologic analysis of 204 patients with a single myocardial infarct. J Am Coll Cardiol. 1986; 7(2):349–354. [PubMed: 2935567]

5. Luckhurst CA, Stein LA, Furber M, Webb N, Ratcliffe MJ, Allenby G, et al. Discovery of isoindoline and tetrahydroisoquinoline derivatives as potent, selective PPARdelta agonists. Bioorg Med Chem Lett. 2011; 21(1):492–446. [PubMed: 21094606]

6. Gorman RC, McCaughan JS, Ratcliffe MB, Gupta KB, Streicher JT, Ferrari VA, et al. Pathogenesis of acute ischemic mitral regurgitation in three dimensions. J Thorac Cardiovasc Surg. 1995; 109(4):684–693. [PubMed: 7715215]

7. Liel-Cohen N, Guerrero JL, Otsuji Y, Handschumacher MD, Rudski LG, Hunziker PR, et al. Design of a new surgical approach for ventricular remodeling to relieve ischemic mitral regurgitation: insights from 3-dimensional echocardiography. Circulation. 2000; 101(23):2756–2763. [PubMed: 10851215]

8. Llaneras MR, Nance ML, Streicher JT, Lima JA, Savino JS, Bogen DK, et al. Large animal model of ischemic mitral regurgitation. Ann Thorac Surg. 1994; 57(2):432–439. [PubMed: 8311608]

9. Zhang P, Guccione JM, Nicholas SI, Walker JC, Crawford PC, Shamal A, et al. Left ventricular volume and function after endoventricular patch plasty for dyskinetic anteroapical left ventricular aneurysm in sheep. J Thorac Cardiovasc Surg. 2005; 130(4):1032–1038. [PubMed: 16214516]

10. Soleimani M, Khazalpour M, Cheng G, Zhang Z, Acevedo-Bolton G, Saloner DA, et al. Moderate mitral regurgitation accelerates left ventricular remodeling after posterolateral myocardial infarction. Ann Thorac Surg. 2011; 92(5):1614–1620. [PubMed: 21945222]

11. Zhang P, Guccione JM, Nicholas SI, Walker JC, Crawford PC, Shamal A, et al. Endoventricular patch plasty for dyskinetic anteroapical left ventricular aneurysm increases systolic circumferential shortening in sheep. J Thorac Cardiovasc Surg. 2007; 134(4):1017–1024. [PubMed: 17903523]

12. Guttman MA, Zerhouni EA, McVeigh ER. Analysis and visualization of cardiac function from MR images. IEEE Computer Graphics and Applications. 1997; 17(1):30–38. [PubMed: 18509519]

13. Ozturk C, McVeigh ER. Four-dimensional B-spline based motion analysis of tagged MR images: introduction and in vivo validation. Physics in Medicine and Biology. 2000; 45(6):1683–1702. [PubMed: 10870718]

14. Wenk JF, Sun K, Zhang Z, Soleimani M, Ge L, Saloner D, et al. Regional left ventricular myocardial contractility and stress in a finite element model of posterobasal myocardial infarction. J Biomech Eng. 2011; 133(4):044501. [PubMed: 21428685]

15. Guccione JM, McCulloch AD, Waldman LK. Passive material properties of intact ventricular myocardium determined from a cylindrical model. J Biomech Eng. 1991; 113(1):42–55. [PubMed: 2020175]

16. Guccione JM, Waldman LK, McCulloch AD. Mechanics of active contraction in cardiac muscle: Part II--Cylindrical models of the systolic left ventricle. J Biomech Eng. 1993; 115(1):82–90. [PubMed: 8445902]

17. Kim YK, Kim SJ, Kramer CM, Yatani A, Takagi G, Mankad S, et al. Altered excitation-contraction coupling in myocytes from remodeled myocardium after chronic myocardial infarction. J Mol Cell Cardiol. 2002; 34(1):63–73. [PubMed: 11812165]

18. Guccione JM, Costa KD, McCulloch AD. Finite element stress analysis of left ventricular mechanics in the beating dog heart. Journal of Biomechanics. 1995; 28(10):1167–1177. [PubMed: 8550635]

19. Sun K, Stander N, Jhun CS, Zhang Z, Suzuki T, Wang GY, et al. A computationally efficient formal optimization of regional myocardial contractility in a sheep with left ventricular aneurysm. J Biomech Eng. 2009; 131(11):111001. [PubMed: 20016753]

20. Wang G, Bergman M, Nguyen A, Turcato S, Swigart P, Rodrigo M, et al. Cardiac transgenic matrix metalloproteinase-2 expression directly induces impaired contractility. Cardiovascular Research. 2006; 69(3):688–696. [PubMed: 16183043]

21. Wang GY, Bergman MR, Nguyen AP, Turcato S, Swigart PM, Rodrigo MC, et al. Cardiac transgenic matrix metalloproteinase-2 expression directly induces impaired contractility. Cardiovasc Res. 2006; 69(3):688–696. [PubMed: 16183043]

22. Cleutjens JP, Verluyten MJ, Smiths JF, Daemen MJ. Collagen remodeling after myocardial infarction in the rat heart. Am J Pathol. 1995; 147(2):325–338. [PubMed: 7639329]

23. Liu J, Wang C, Murakami Y, Gong G, Ishibashi Y, Prody C, et al. Mitochondrial ATPase and high-energy phosphates in failing hearts. Am J Physiol Heart Circ Physiol. 2001; 281(3):H1319–H1326. [PubMed: 11514303]

24. Zhang Z, Sun K, Saloner DA, Wallace AW, Ge L, Baker AJ, et al. The benefit of enhanced contractility in the infarct borderzone: a virtual experiment. Front Physiol. 2012; 3:86. [PubMed: 22509168]

25. Best PM. Cardiac muscle function: results from skinned fiber preparations. Am J Physiol. 1983; 244(2):H167–H177. [PubMed: 6401938]

26. Stephenson EW. Activation of fast skeletal muscle: contributions of studies on skinned fibers. Am J Physiol. 1981; 240(1):C1–C19. [PubMed: 6257114]

27. Rodriguez F, Langer F, Harrington KB, Cheng A, Daughters GT, Criscione JC, et al. Alterations in transmural strains adjacent to ischemic myocardium during acute midcircumflex occlusion. J Thorac Cardiovasc Surg. 2005; 129(4):791–803. [PubMed: 15821645]

28. Langer F, Rodriguez F, Cheng A, Ortiz S, Harrington KB, Zasio MK, et al. Alterations in lateral left ventricular wall transmural strains during acute circumflex and anterior descending coronary occlusion. Ann Thorac Surg. 2007; 84(1):51–60. [PubMed: 17588382]

29. Wilson EM, Moainie SL, Baskin JM, Lowry AS, Deschamps AM, Mukherjee R, et al. Region- and type-specific induction of matrix metalloproteinases in post-myocardial infarction remodeling. Circulation. 2003; 107(22):2857–2863. [PubMed: 12771000]

30. Mukherjee R, Mingoia JT, Bruce JA, Austin JS, Stroud RE, Escobar GP, et al. Selective spatiotemporal induction of matrix metalloproteinase-2 and matrix metalloproteinase-9 transcription after myocardial infarction. Am J Physiol Heart Circ Physiol. 2006; 291(5):H2216–H2228. [PubMed: 16766634]

31. Sawicki G, Leon H, Sawicka J, Sariahmetoglu M, Schulze CJ, Scott PG, et al. Degradation of myosin light chain in isolated rat hearts subjected to ischemia-reperfusion injury: a new intracellular target for matrix metalloproteinase-2. Circulation. 2005; 112(4):544–552. [PubMed: 16027249]

32. Gao CQ, Sawicki G, Suarez-Pinzon WL, Csont T, Wozniak M, Ferdinandy P, et al. Matrix metalloproteinase-2 mediates cytokine-induced myocardial contractile dysfunction. Cardiovasc Res. 2003; 57(2):426–433. [PubMed: 12566115]

33. Carrick R, Ge L, Lee LC, Zhang Z, Mishra R, Axel L, et al. Patient-specific finite element-based analysis of ventricular myofiber stress after Coapsys: importance of residual stress. Ann Thorac Surg. 2012; 93(6):1964–1971. [PubMed: 22560323]

34. Wall ST, Walker JC, Healy KE, Ratcliffe MB, Guccione JM. Theoretical impact of the injection of material into the myocardium: a finite element model simulation. Circulation. 2006; 114(24): 2627–2635. [PubMed: 17130342]

35. Rice JJ, Wang F, Bers DM, de Tombe PP. Approximate model of cooperative activation and crossbridge cycling in cardiac muscle using ordinary differential equations. Biophys J. 2008; 95(5):2368–2390. [PubMed: 18234826]
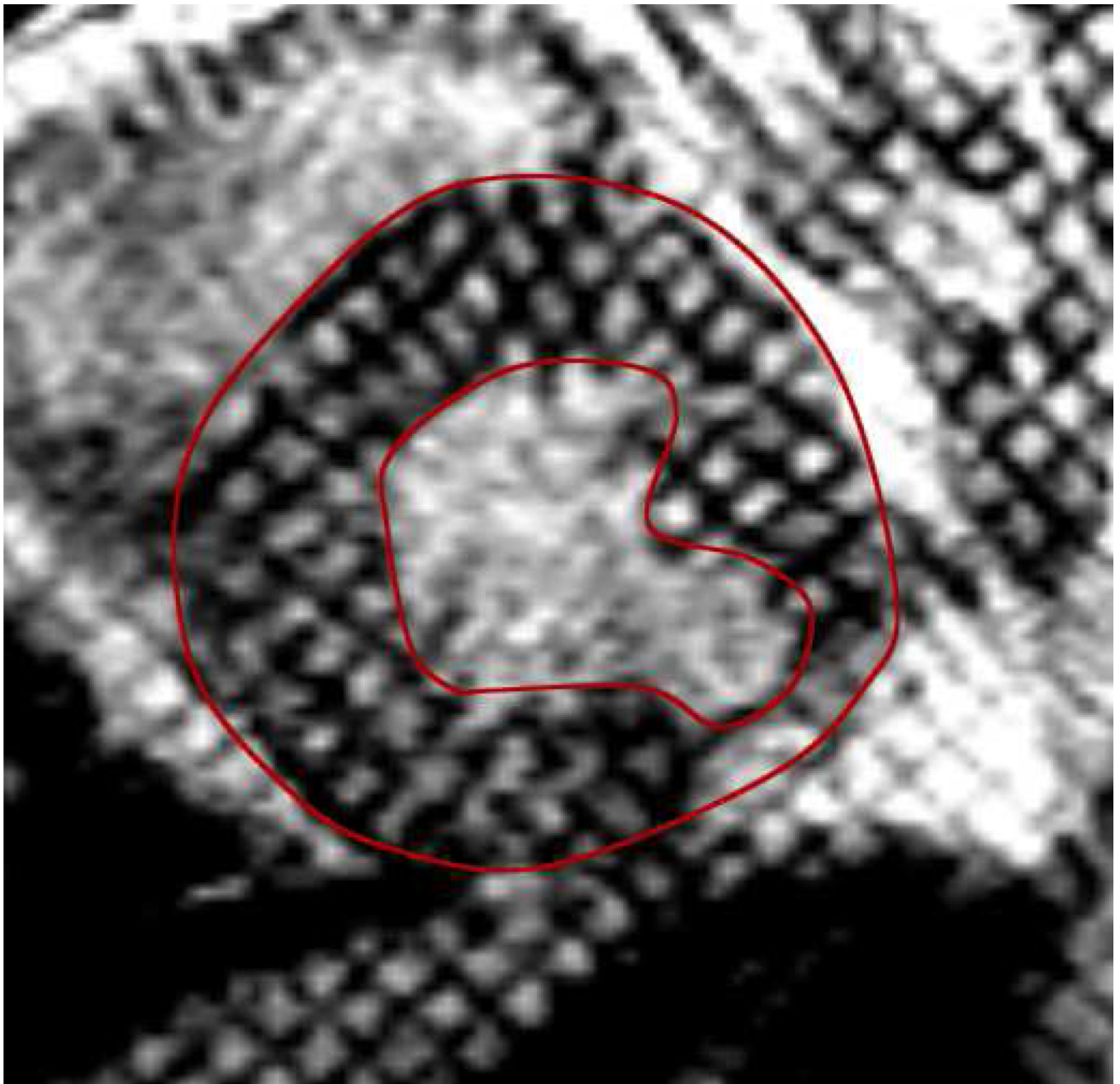
Figure 1.
Example of an *in vivo* tagged short axis MRI image of the sheep left ventricle with a postero-lateral myocardial infarction (16 weeks post-MI). The epicardial and endocardial contours are traced in red. Notice the thinned wall of the infarcted region.
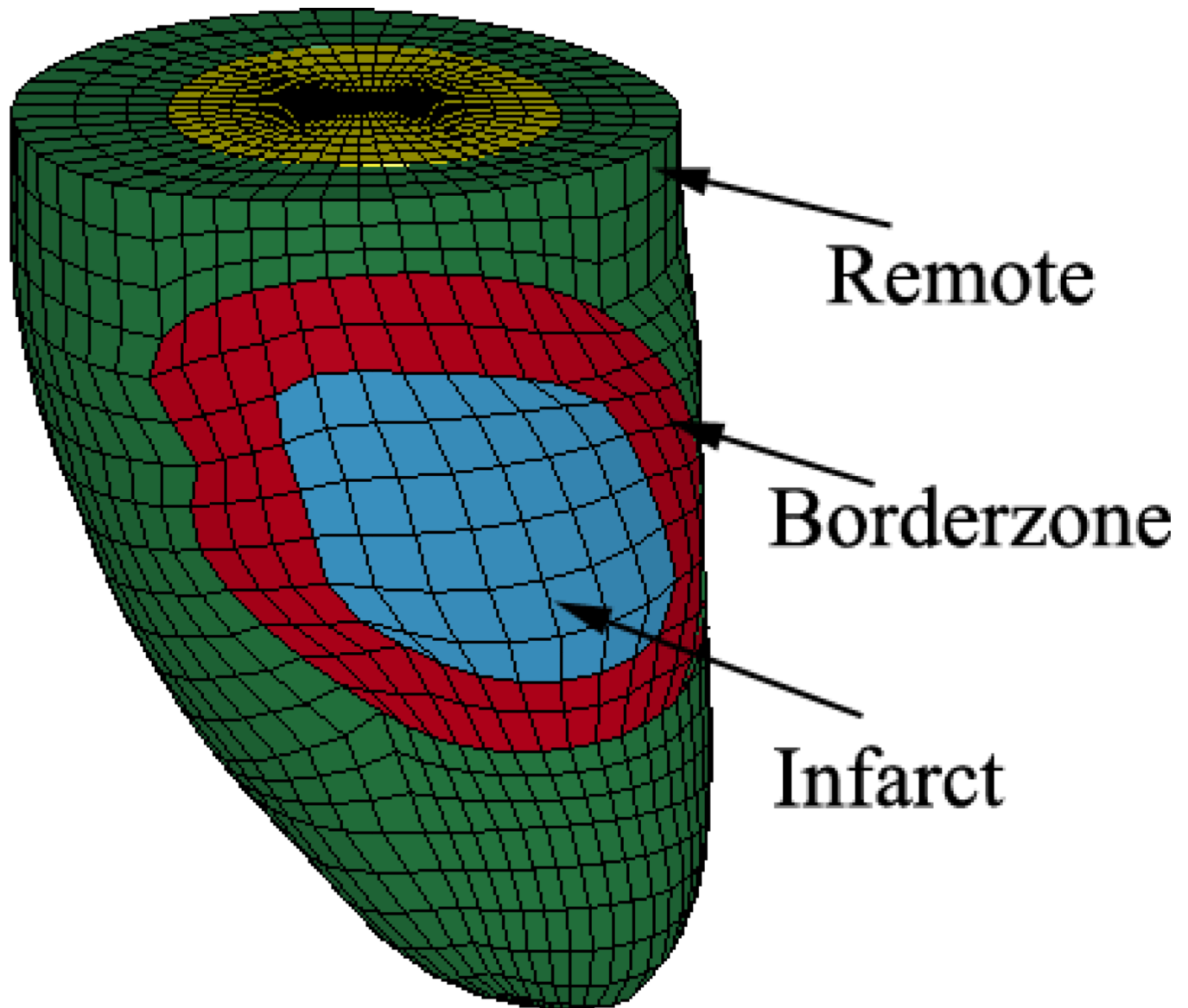
Figure 2.
Example of an animal-specific finite element model of the sheep left ventricle with a postero-lateral myocardial infarction (16 weeks post-MI) showing the spatial distribution of the infarct (blue), borderzone (red) and remote (green) regions in the 3D mesh.
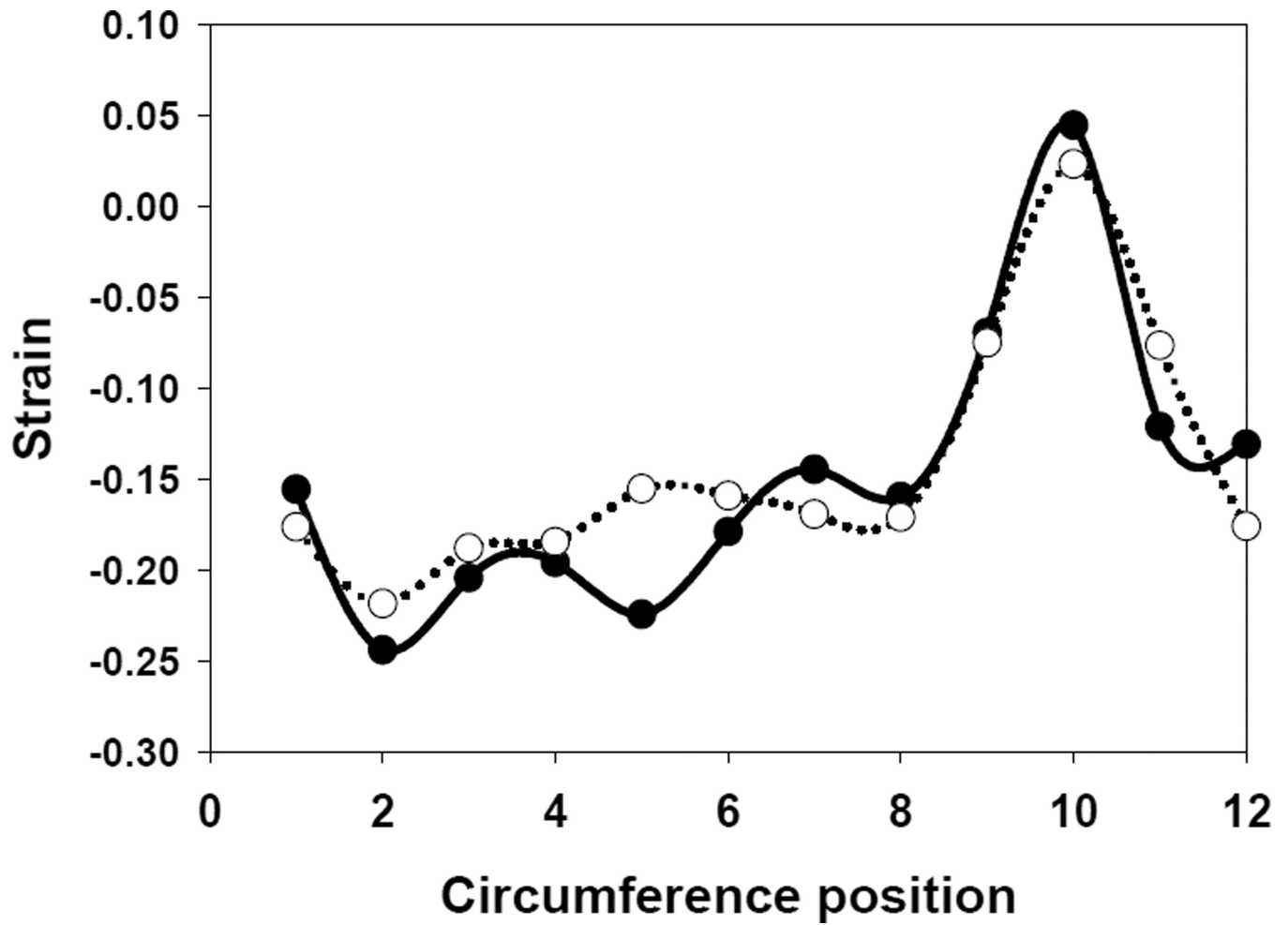
Figure 3.
Example circumferential strain distribution in a single short axis slice of a post-MI left ventricle, showing both experimental and FE predicted results.
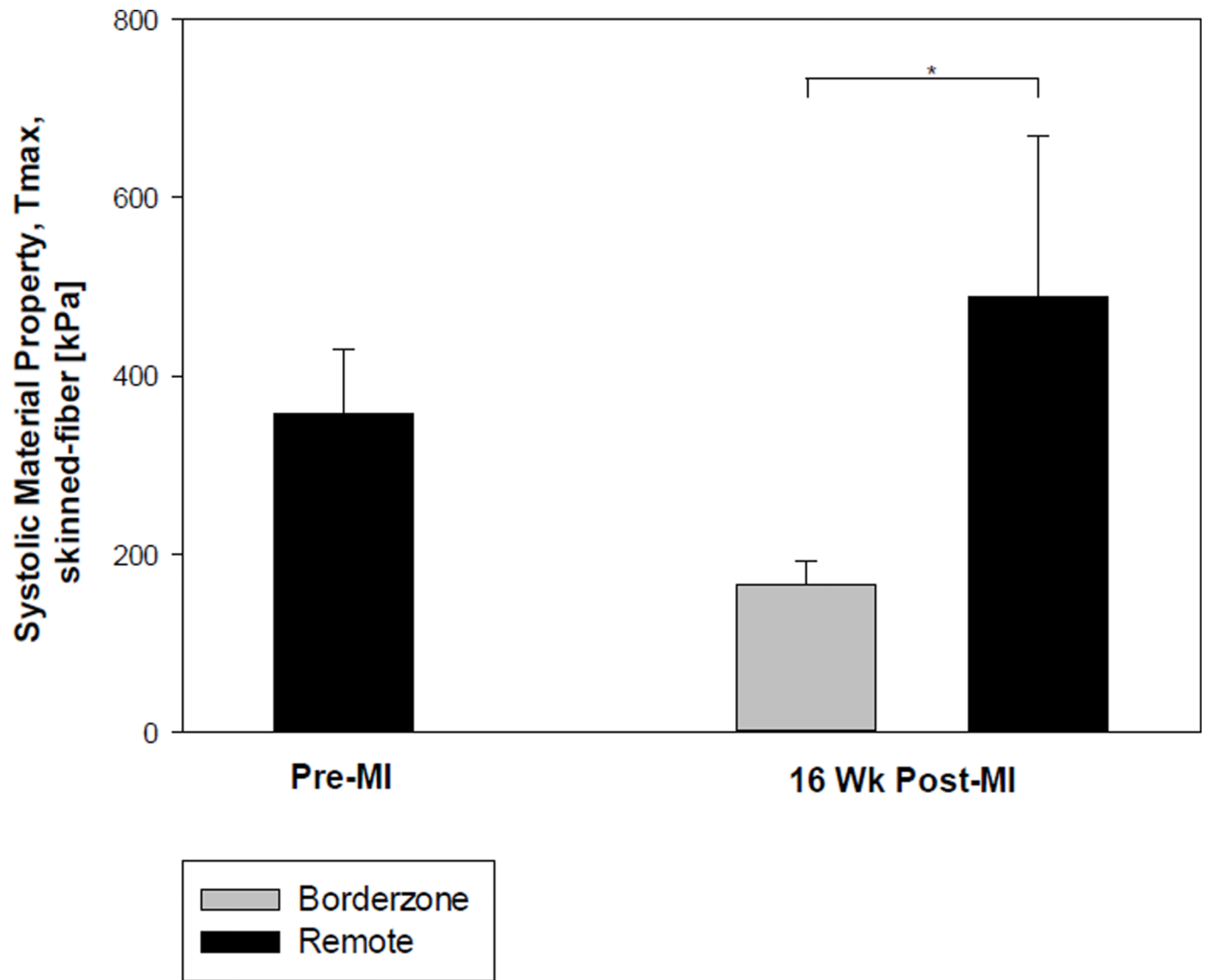
Figure 4.
FE model systolic material property (T_{max}) before creation of MI, and in the borderzone and remote region 16 weeks after postero-lateral MI in sheep. $n=5$, $*p<0.05$.
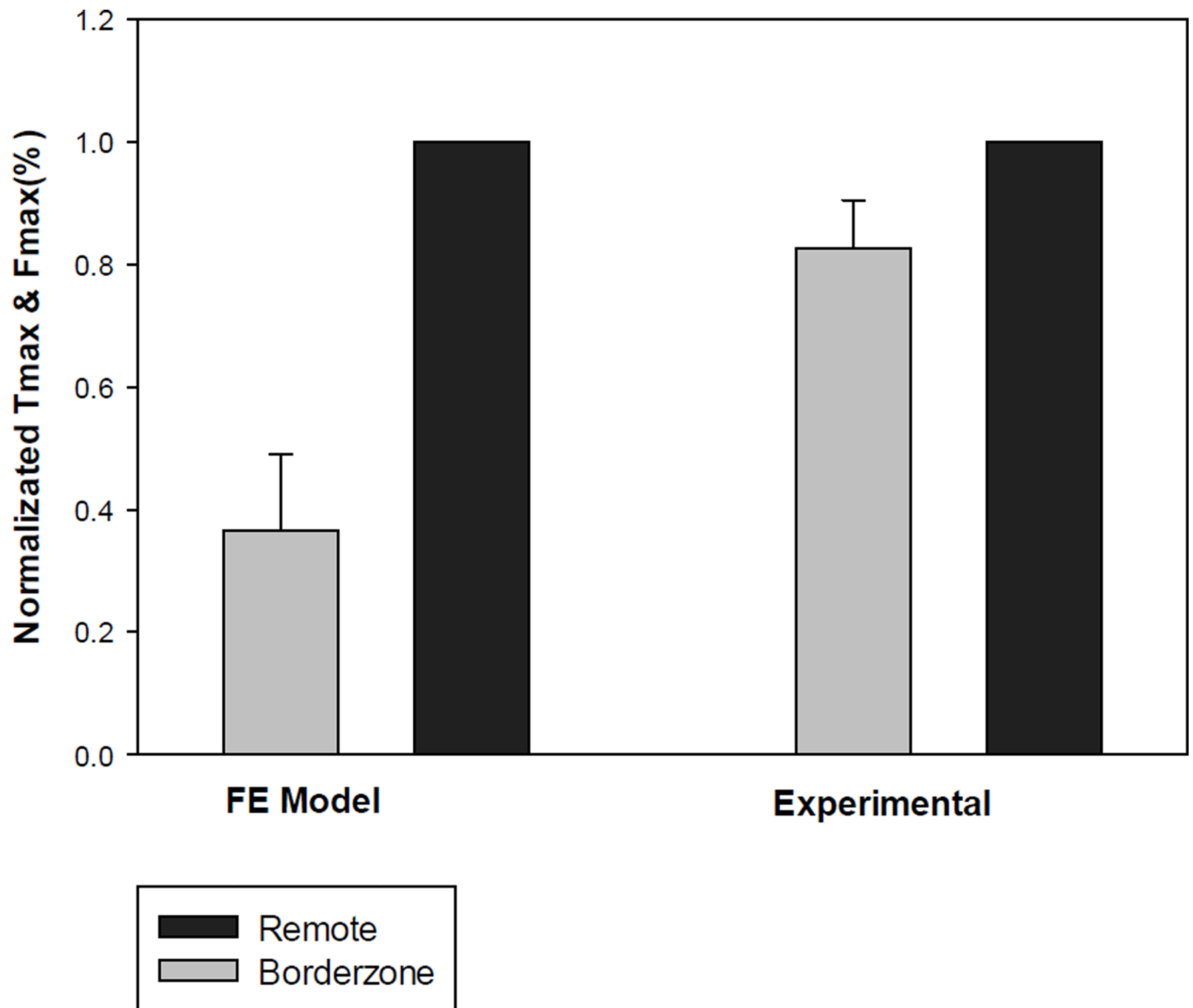
Figure 5.
FE model systolic material property (T_{max}) and experimentally-measured maximum skinned fiber contractile force (F_{max}) normalized to respective remote myocardium 16 weeks after postero-lateral MI in sheep. N=5 for all groups. *p<0.05.
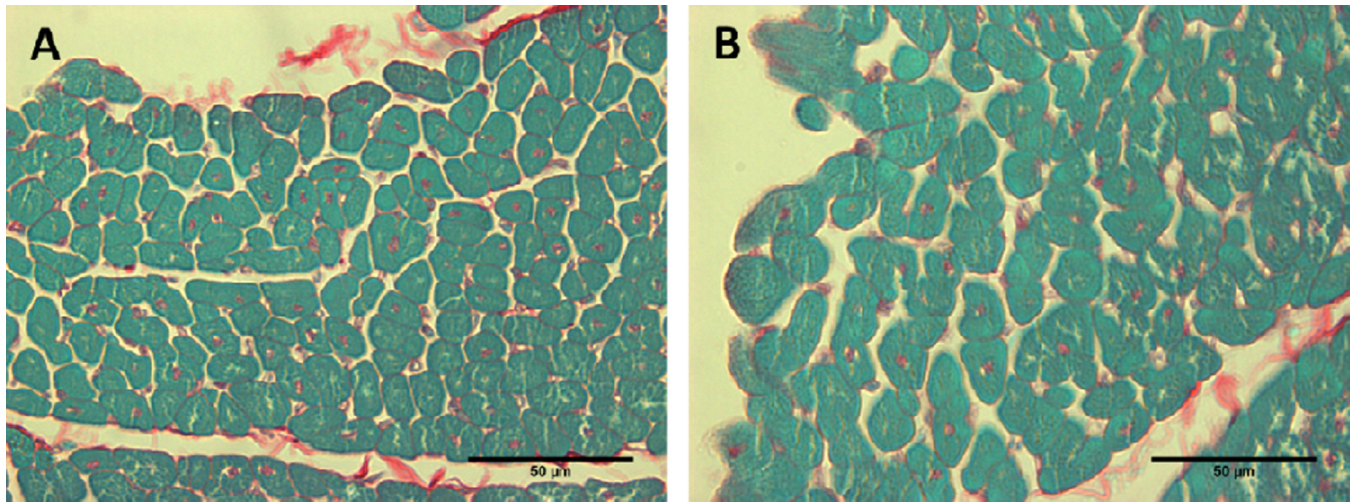
Figure 6.
Representative picrosirius red-stained histological sections of sheep remote (A) and borderzone (B) myocardium, showing myocyte hypertrophy in the BZ. No appreciable difference in collagen content is observed between the remote myocardium and BZ. Scale bar is 50 μm.

Table 1

Effect of Ischemic MR on left ventricular pressure and volume. Values are mean ± standard deviation. LVP = left ventricular pressure; VED = end-diastolic volume; VES = end-systolic volume; SV = stroke volume; EF = ejection fraction.

	Before MI (*n*=5)	16 weeks after MI (*n*= 5)	*p*
LVP at ED [mmHg]	7.68 ± 3.32	7.16 ± 1.98	0.7755
LVP at ES [mmHg]	89.54 ± 4.68	88.52 ± 4.34	0.7309
VED [ml]	104.7 ± 7.8	130.2± 33.9	0.1522
VES [ml]	49.6 ±6.3	74.5 ± 24.8	0.0788
SV [ml]	54.0 ± 6.0	55.7 ± 14.2	0.8099
Forward SV [ml]	56.4± 8.6	40.4 ± 11.1	0.033
EF [%]	51.2± 3.4	43.2 ± 8.5	0.0954

Table 2

Experimental and FE predicted circumferential strain, shown by time point and region.

		Remote	BZ	Infarct
Pre-MI	Experimental	−0.13408		
		± 0.01846552		
	Predicted	−0.13021		
		± 0.02438154		
16 weeks after MI	Experimental			
		−0.08683	−0.05437	−0.03449
		± 0.00897124	± 0.031606945	± 0.042061607
	Predicted	−0.11294	−0.01940	0.06857
		± 0.03091068	± 0.02487941	± 0.029879206

Table 3

F_{max} measured *in vitro* using skinned myocardial fibers.

	Passive tension = 0.98 mN/mm^2 (*n*=3) [mN/mm^2]	Sarcomere length = 2.1 μm (*n*=2) [mN/mm^2]
Remote Zone	35.93 ± 4.63	82.50 ± 2.51
Borderzone	28.79 ± 5.49*	68.45 ± 0.21
p	0.029	0.086